Antenna Design in Radio Communications, Radio Astronomy and Astroparticle Physics Applications

Jorge Torres

PhD Candidacy Written Examination

Department of Physics

The Ohio State University

Candidacy committee:

Prof. Amy Connolly, Chair

Prof. John Beacom

Prof. Jim Beatty

Prof. Rolando Valdés-Aguilar

August 6, 2017

Contents

1 Introduction

Antennas are devices that emit and receive radiation that can travel in media. Through this phenomenon, information can be transmitted/received, which is of interest for many applications. The most common application is communication and the wireless internet is a notable example. However, other non-ordinary uses of antennas exist. For example in radio astronomy and astroparticle physics, which, besides communications, are the topics we will cover in this work. An emphasis on astroparticle physics will be made.

For each practical use of an antenna, the design of such devices often varies. One of the reasons, usually the main one, for this is that the desired signal to be detected/emitted has different characteristics. Similarly, mechanical requirements could be necessary, such that the antenna can endure the conditions at which it will be put through. In this work we will introduce some of the parameters used to evaluate the performance of an antenna, with a concentration on those used for receiving antennas.

For each of the three fields of application: communication, radio astronomy and astroparticle physics, we will discuss how the particular needs of each of those shape the design of the antenna, providing some current and future efforts aimed at the improvement of antenna design. Additionally, in the astro particle physics section we will superficially explain the generation of the radio signals that need to be detected, and will limit our scope to some of the current ultra-high energy neutrino (UHE-ν) experiments that use antennas to detect such signal, concluding, as in the other sections, with current efforts and future prospects.

2 Fundamentals of Antenna Theory

In order to be able to design an antenna, one must know the physical principles behind them, and the parameters that are used to evaluate their performance. In this section, we will concisely describe the physics underlying radiation and its relation to antennas, and some of the parameters used to describe antenna performance, focusing on those relevant to receiving antennas.

2.1 The physics of antennas

A time-changing system of charges and currents produces electromagnetic radiation. This is the physical principle behind electromagnetic emission by antennas. To see this, consider a localized system of charges that vary sinusoidally in time

$$\begin{aligned} \rho(\boldsymbol{x}, t) &= \rho(\boldsymbol{x}) e^{-i\omega t} \\ \boldsymbol{J}(\boldsymbol{x}, t) &= \boldsymbol{J}(\boldsymbol{x}) e^{-i\omega t} \end{aligned} \tag{2.1}$$

where $\rho(\boldsymbol{x}, t)$ is the charge density, $\boldsymbol{J}(\boldsymbol{x}, t)$ is the current density, and ω is the oscillation frequency.

In electromagnetic theory, a system can be described by its electric and magnetic fields, both of which are derived from the vector potential. To describe the vector potential, let us assume the sources to be in empty space with no boundary surfaces, and the electromagnetic potentials and fields to have the same time dependence. In the Lorenz gauge, this potential has the form [31]:

$$\boldsymbol{A}(\boldsymbol{x}) = \frac{\mu_0}{4\pi} \int d^3x' \boldsymbol{J}(\boldsymbol{x'}) \frac{e^{ik|\boldsymbol{x}-\boldsymbol{x'}|}}{|\boldsymbol{x}-\boldsymbol{x'}|}, \tag{2.2}$$

where $k = \omega/c$ is the wave number, μ_0 is the vacuum permeability, and the primed and unprimed coordinates denote the coordinates from the origin to the charge distribution, and from the origin to and observer, respectively. Also, a sinusoidal time dependence is implicit.

We are interested in the limit that the source is confined to a very small region, much less than a wavelength λ. Let us also assume an observer in the far (radiation) zone, i.e., $d \ll \lambda \ll r$, where d is the size of the source, $\lambda = 2\pi c/\omega$ is the wavelength, and r is the distance between the observer and the source. From [31], the vector potential in the far zone is

$$\boldsymbol{A_{far}}(\boldsymbol{x}) = \frac{\mu_0}{4\pi} \frac{e^{ikr}}{r} \int d^3x' \boldsymbol{J}(\boldsymbol{x'}) e^{-ik\boldsymbol{n}\cdot\boldsymbol{x'}}, \tag{2.3}$$

where $\boldsymbol{n}$ is a unit vector in the direction of $\boldsymbol{x}$. From Eqn. (2.3), the vector potential falls off as r^{-1}, and has angular dependence $(\boldsymbol{n} \cdot \boldsymbol{x'})$. Thus, $\boldsymbol{A_{far}}$ behaves as an outgoing spherical wave.

The electric and magnetic fields hold onto this $1/r$ dependence, and both of them are transverse to the direction of propagation. They thus correspond to radiation fields.

This principle can be reversed, allowed due to time-invariance of Maxwell's equations, to study receiving antennas.

2.2 Important antenna parameters

There are many factors that influence the performance of an antenna, and that are of great importance when designing a device for a particular task. In this subsection we will describe the most important ones regarding receiving antennas. Definitions in quotation marks are from the *IEEE Standard for Definitions of Terms for Antennas* [1].

2.2.1 Radiation pattern

The radiation pattern is "the spatial distribution of a quantity that characterizes the electromagnetic field generated by an antenna." There are two kinds of antennas distinguished by their radiation pattern: an isotropic antenna is an ideal lossless antenna whose radiation pattern is rotationally and radially invariant. On the other hand, a directional antenna is one " having the property of radiating or receiving electromagnetic waves more effectively in some direction(s) than others."

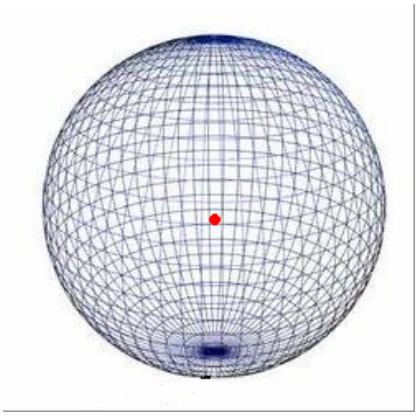

(a) Isotropic (ideal) antenna. Although no isotropic antenna exists, the closest device to it is a dipole antenna.

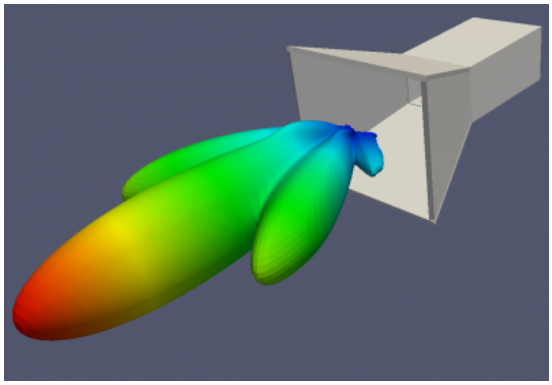

(b) Directional (horn-type) antenna. Note that there is one main lobe, and two side lobes. The side lobes represent unwanted radiation in undesired directions.

Figure 1: Radiation patterns for an isotropic and a directional antenna.

For linearly polarized antennas, two useful features for describing their performance are the principal E- and H-plane beam patterns. The E-plane is defined as "the plane containing the electric-field vector and the direction of maximum radiation", and the H-plane as "the plane containing the magnetic-field vector and the direction of maximum radiation."

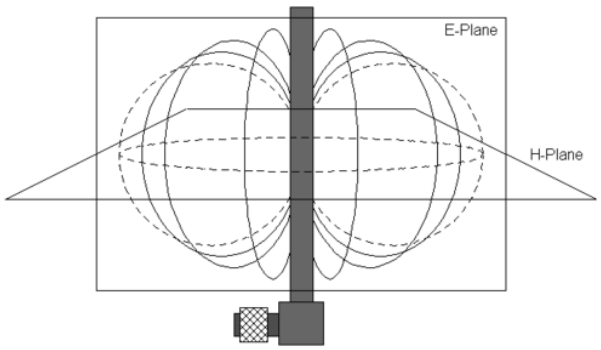

Figure 2: The E- and H- fields for a vertically polarized dipole antenna.

2.2.2 Gain

The gain is "the ratio of the radiation intensity in a given direction to the radiation intensity that would be produced if the power accepted by the antenna were isotropically radiated." Mathematically, the gain factor is

$$G = 4\pi \frac{U(\theta, \phi)}{P_{in}(\text{lossless isotropic source})}, \tag{2.4}$$

where $U(\theta, \phi)$ is the radiated power per solid angle of the antenna, and P_{in} is the total input power.

Gain is usually expressed in dBi, scaled with respect to an ideal, isotropic radiator. The gain of an antenna in dBi can be found from the gain factor as follows:

$$G_{\text{dBi}} = 10 \cdot \log_{10}(G). \tag{2.5}$$

For example, an antenna of gain factor $G = 2$, meaning that the antenna emits/receives twice the power relative to an isotropic antenna, has a gain of $\sim$3 dBi.

2.2.3 Efective area

The effective area is "in a given direction, the ratio of the available power at the terminals of a receiving antenna to the power flux density of a plane wave incident on the antenna from that direction, the wave being polarization matched to the antenna. If the direction is not specified, the direction of maximum radiation intensity is implied." This area is related to the gain G as follows:

$$A_e = \frac{P}{S} = \frac{G\lambda^2}{4\pi}, \tag{2.6}$$

where $\lambda = c/\nu$ is the wavelength, and S is the Poynting vector. In other words, the output power of an antenna in watts (W) is equal to the power density of the radio waves (W/m^2) multiplied by its aperture (m^2): $P = A_e \cdot S$.

2.2.4 Effective height

A receiving antenna captures electromagnetic waves, which need to physically hit it, and extracts power from them by converting it to a voltage induced on the open-circuit terminals of the antenna. There are antennas which are not defined by a physical area, e.g., monopoles and dipoles, and thus cannot be characterized by an effective area. For them, the effective height $\boldsymbol{h_e}$ plays an analogous role as the effective area for aperture antennas and it helps to characterize the degree of polarization mismatch that may exist between the incident field and the antenna. $\boldsymbol{h_e}$ is a complex vector in the $\theta\phi$-plane:

$$\boldsymbol{h_e}(\theta, \phi) = \hat{\boldsymbol{e}}_{\boldsymbol{\theta}} h_\theta(\theta, \phi) + \hat{\boldsymbol{e}}_{\boldsymbol{\phi}} h_\phi(\theta, \phi), \tag{2.7}$$

and its magnitude is given in meters.

Let $\boldsymbol{E}$ be the incident electric field, and V_{oc} be the open circuit voltage at antenna terminals. The vector effective height $\boldsymbol{h_e}$ is related to the last two quantities in the following way:

$$V_{oc} = \boldsymbol{E} \cdot \boldsymbol{h_e} \tag{2.8}$$

Note that no voltage is induced if the polarizations of the antenna and the electric field are

orthogonal to each other.

2.2.5 VSWR

The voltage standing wave ratio (VSWR) relates the reflected power P_R to the transmitted power P_T on an antenna in the following way:

$$\frac{P_R}{P_T} = \left(\frac{\text{VSWR} - 1}{\text{VSWR} + 1}\right)^2. \tag{2.9}$$

VSWR also satisfies the following:

$$\text{VSWR}(\nu) = \frac{|\rho(\nu) + 1|}{|\rho(\nu) - 1|}, \tag{2.10}$$

where $\rho(\nu)$ is the complex voltage coefficient of the antenna (the ratio of the electric field strength of the reflected wave to that of the incident wave) and is related to the effective power transmission coefficient T as follows

$$T(\nu) = |1 - \rho(\nu)|^2. \tag{2.11}$$

VSWR= 1 denotes full transmission of the wave (no reflections), as can be seen from Eq. 2.11, and thus no standing wave along the transmission line[1]. On the other hand, very high values mean high reflection and standing wave behavior along the transmission line.

2.2.6 Antenna temperature

Every object whose temperature is not zero Kelvin emits radiation described by Planck's law. This radiation can be intercepted by an antenna, creating unwanted noise. The quantification of this noise is important, as it could be greater than the expected signal, and we describe it below.

Consider an antenna of narrow beam whose pattern is confined to a solid angle $d\Omega$ and is

[1] A transmission line is the device (usually a coaxial cable) used to transmit radio frequency energy between the antenna and the radio receiver/transmitter.

pointed toward the (θ, ϕ) direction. The received power in $d\Omega$ is

$$\frac{dP_{\text{rec}}}{d\Omega} = \frac{k_B T(\theta,\phi) G(\theta,\phi) \Delta\nu}{4\pi}, \tag{2.12}$$

where $T(\theta, \phi)$ is the temperature of the source at those angles, $G(\theta, \phi)$ is the gain, k_B is the Boltzmann constant, and $\Delta\nu$ is the frequency bandwidth of the receiver. Integrating over all the angles yields the total received power:

$$\begin{aligned} P_{\text{total}} &= \frac{k_B \Delta\nu}{4\pi} \int_{4\pi} G(\theta,\phi) T(\theta,\phi) d\Omega \\ &= k_B \Delta\nu T_{\text{ant}}, \end{aligned} \tag{2.13}$$

where

$$T_{\text{ant}} = \frac{1}{4\pi} \int_{4\pi} G(\theta,\phi) T(\theta,\phi) d\Omega. \tag{2.14}$$

This parameter describes how much noise an antenna produces in a given environment, and does not represent the physical temperature of the antenna. Significant contributions to the antenna temperature can come from small GT products over large areas (low-gain antennas looking all over the sky), or large GT products over small areas (high-gain antennas looking over a small area).

2.2.7 Signal-to-noise ratio (SNR)

The signal-to-noise ratio is defined as the ratio of the signal voltage to the thermal noise voltage. Here we derive the SNR in terms of other antenna parameters.

The expected signal strength E_0 induces a voltage at the antenna receiver given by[2]

$$V_s = h_e E_0 \Delta\nu. \tag{2.15}$$

Kraus [33] derives the following expression for the antenna effective height h_e

$$h_e = 2\sqrt{\frac{Z_a \eta A_e}{Z_0}} \cos\theta_p, \tag{2.16}$$

[2]The units of E_0 are given in the Fourier domain [V/m/Hz].

where Z_a is the antenna radiation resistance, η is the antenna efficiency, A_e is the effective area, $Z_0 = 377\,\Omega$ is the impedance of free space, and θ_p is the polarization angle of the antenna with respect to the plane of polarization of the radiation. Thus,

$$V_s = 2\sqrt{\frac{Z_a \eta A_e}{Z_0}} \cos\theta_p E_0 \Delta\nu. \tag{2.17}$$

Similarly, from the fact that $P = \frac{E^2 A_e}{Z_0}$ (cf. Eq. 2.6) and Eq. 2.13, one can get the average thermal noise voltage in the system

$$V_n = \sqrt{4 k_B T_{\text{ant}} Z_a \Delta\nu}. \tag{2.18}$$

Thus, the SNR is

$$SNR \equiv \frac{V_s}{V_n} = E_0 \cos\theta_p \sqrt{\frac{\eta A_e \Delta\nu}{k_B T_{\text{ant}} Z_0}}. \tag{2.19}$$

One can find the minimum detectable field strength by setting SNR=1 in the last equation and solving for E_0.

3 Antennas and their Applications to Communications, Radio astronomy and Astroparticle Physics

Antennas can be used to both transmit and receive electromagnetic signals, which can be translated into information, and thus they play a very important role in the world of communication. Therefore, antennas are found in every wireless device such as televisions, cellphones, computers, and a vast amount of other devices that emit and/or receive information.

Besides technological applications, antennas are useful in the physics research world. We will concentrate on two fields of physics that make use of antennas: radio astronomy and astroparticle physics. Those fields use antennas to study the cosmos, and as particle detectors, respectively.

3.1 Communication: antennas as information exchange devices

Communication was the first application that antennas had. In the 19th century, Marconi and Hertz were the first to realize the practical applications of radio waves in communication. Significant evolution has occurred since then. Now it is possible to quickly exchange large amounts of data from small devices.

Due to its rapid adaptation to human necessities, an extensive variety of antennas have been created; varying in size, shape and other features in order to fit into devices, or perform specific tasks. For this particular work, we will focus on the paraboloidal antenna, since it can be found in both communications and radio astronomy. For the field of communications, we will concentrate on antennas used in spacecrafts, principally paraboloidal reflectors.

3.1.1 The paraboloidal reflector

From the physical and geometrical point of view, if a wave is incident on a paraboloidal surface, it will be concentrated in a point called the focus, which is equidistant to any point on the paraboloidal surface. The geometry of a paraboloidal reflector antenna is wholly described by its focal length and its radius. This gives us insight to the physical significance of a paraboloidal antenna, where a bundle of light rays incident on such antenna will be collimated into the focus, adding the field contributions in phase.

There are many design criteria to be considered in order to maximize the efficiency of a paraboloidal reflector antenna. We will give a brief description of them as follows[3]:

- **illumination**: at its focal point, the reflector has a feed antenna that emits and receives radiation, and it has to have a certain size to efficiently observe/illuminate the reflector. This *illumination efficiency* depends on the radiation pattern of the feed and describes the ratio of *illuminated area* to the physical area. Common feeds are horns, dipoles and helices.

- **spillover**: the amount of radiation that "spills over" the edge of the reflector and gets dispersed. It is defined by [1] as "in the transmitting mode of a reflector antenna, the

[3]They are extensively and quantitatively discussed in [8, 36]

power from the feed that is not intercepted by the reflecting elements."

- **electrical resistance**: radiation resistance + ohmic resistance (loss). Determined by the geometry and material composition of the antenna.
- **surface errors**: deviations from a perfectly paraboloidal surface.
- **focus**: errors due to the feed not being placed at the focal point.
- **blocking**: loss of efficiency caused by the shadowing on the reflector by feed and its support.

(a) A parabolic antenna.

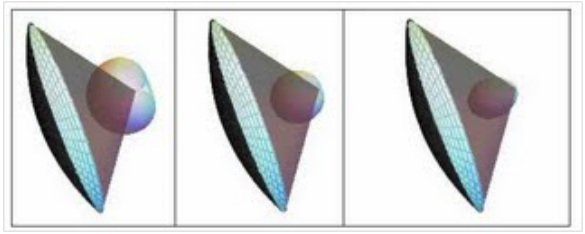

(b) Graphic demonstration of the spillover effect. Antenna feeds with higher gains help radiation to be emitted within the angle of the dish.

Figure 3

Paraboloidal reflectors are directional (high-gain) antennas, meaning they receive/radiate greater power preferentially. For antennas used in spacecrafts, high gain is the prime feature, as these devices must be accurately directed at a station on the ground or a satellite. Also, the antenna has to be resistant to all the inclemencies suffered by a spacecraft, and be of a size adequate for the vehicle.

In addition to design criteria regarding reflector antennas, other considerations (intrinsic to antennas for spacecrafts) concerning the feed must also be taken into account. This is one of the most challenging parts of the design, as antenna reflectors used in spacecrafts often have to emit/receive in multiple polarizations and at a range of frequencies due to the nature of the

transmitted information [30]. The very particular specifications of the spacecraft antenna make it very difficult to design. Also, some of the antenna parameters such as the beam pattern cannot be analytically calculated. Instead one must use numerical methods to describe it, which could be time and labor intensive. This is why (super)computers and algorithms play a very important role on antenna design.

3.1.2 Current efforts

Computational electrodynamics helps to model the interaction of EM fields with antennas and other objects, and then optimize their design. Examples of this tool are the *Numerical Electromagnetic Code* (NEC) and the *High Frequency Structural Simulator* (HFSS). Other methods to design and optimize antennas have been born along due to technological advances, like genetic programming. The antenna prototypes designed with genetic algorithms (GA) are called *evolved antennas*, and they have been studied since the early 1990s. Roughly, GAs heuristically search the most fit hypothesis with respect to some desired parameters from a pool of possible solutions, following the natural process of evolution. As an example of this, we take the work done by Lohn *et al* [35] (not a reflector antenna). They developed an evolved antenna that had to meet a specific set of mission requirements to be deployed on a spacecraft. Particularly, a combination of wide beamwidth for a circularly-polarized wave and wide bandwidth, but also with VSWR, size, shape and weight limitations. The resulting antenna was compliant with respect to the performance requirements, and it had a shorter design cycle. Furthermore, it had additional advantages to the conventionally-designed antenna such as potential power saving and more uniform coverage of the desired area.

The use of supercomputers has permitted the acceleration of these simulations and increase their precision significantly. Also, other machine learning tools have appeared, paving the way for better optimization and design of antennas. This has not only been applied on the communications side, but also in other fields as we will see later.

3.2 Radio astronomy: antennas as telescopes

Research on communication antennas by Karl Guthe Jansky led him to discover radio emission from the Milky Way in 1931, giving birth to what is known today as radio astronomy. Coincidently, the Earth's atmosphere is transparent to a broad range of radio wavelengths, being bounded in the upper edge by absorption and reflection by the ionosphere (dominant at frequencies $\lesssim 10$ MHz), and atmospheric molecular absorption bands in the lower edge (the boundary between the radio and far-infrared regimes), permitting the study of radio waves emitted by galactic and extragalactic sources. Thanks to radio astronomy, the discovery of the cosmic microwave background radiation, associated to the Big Bang Theory, was made. Currently, radio techniques and antennas are regarded as some of the most important tools available to radio astronomy for studying the universe, addressing a broad range of phenomena, such as synchrotron radiation, which was the source of the radiation that Jansky discovered, and thermal radiation from a wide variety of thermal regimes.

In radio astronomy, antennas get a fancier name: radio telescopes. These devices have two basic requirements: sensitivity, which is the ability to distinguish between a signal from noise, and angular resolution, which is the capacity to distinguish small details of an object. Both of these fundamental parameters depend on the size of the telescope aperture; sensitivity depends on the total collecting area (cf. SNR, Eq. 2.19), while angular resolution depends on the overall dimensions of a telescope[4]. Sensitivity is important because radio-band radiation incident on the Earth is very weak. For example, the power flux density at Earth of a quiet sun is about 10^6 *jansky* (Jy) [34], where 1 Jy$= 10^{-26} \cdot \mathrm{W} \cdot \mathrm{m}^{-2} \cdot \mathrm{Hz}^{-1}$. The sensitivity problem can thus be addressed by constructing large effective area antennas. These antennas need to be steerable if they are directional to be useful as radio telescopes. Paraboloidal reflector antennas are often the first choice.

In this section, we will concentrate on three different telescope categories: single-dish (-aperture) antennas, phased arrays, and interferometers.

[4]The angular resolution θ(radians) can be approximated by $\theta = \frac{\lambda}{D}$, where D is the diameter of the dish.

3.2.1 Single-aperture antennas

These antennas have large dish-shaped reflectors in order to maximize directivity, which subsequently increases the sensitivity of the telescope. Examples of single aperture antennas are The Green Bank Telescope in West Virginia (USA), the Arecibo telescope (Puerto Rico), Effelsburg (Germany), Jodrell Bank (England), Parkes (Australia), and others. This category also include millimetre and sub-millimetre telescopes, whose dimensions are smaller than that of those previously described, targeted at smaller wavelengths.

The latest developments in this category include offset-fed systems, where the antenna feed is offset to the side of the reflector, which have not been consistently incorporated due to their considerable cost and complexity, and the adoption of phased array feeds (PAFs). A PAF is a feed, located at the focus of the paraboloidal reflector, consisting of an array of a large number of low-gain antennas which are combined to form beams [19], which are directional projections of radiation. Beamforming is useful because the radio telescopes can achieve spatial selectivity. Also, beams can be individually controlled, which cannot be done with traditional array receivers.

Regarding angular resolution, diffraction is very important and must be understood in terms of wavefronts at the telescope aperture. In practice, the angular resolution of single-aperture radio telescopes is not adequate and one must draw on interferometer techniques, which will be discussed later.

3.2.2 Phased arrays

The radio spectrum ranges from millimeters to hundreds of kilometers. It is difficult for a single antenna to cover the totality of such spectrum, especially for the longest wavelengths, as the sensitivity is limited by the size of the dish, which in turn is limited by mechanical features. For this case, it is possible to use flat arrays of lower-gain dipole elements or dishes of smaller area than single-aperture telescopes distributed over the ground, spanning a larger area than what could be achieved with a single, large antenna. This arrangement of antennas is known as a phased array. For wavelengths $\gtrapprox$ 1 m it becomes practical and economic to use large numbers of lower-gain elements instead of reflector antennas, as they are cheaper and easier to

deploy than reflectors. The reasons for this are that at these wavelengths small paraboloidal reflectors have poor directivity, and the antenna temperature dramatically increases with both gain ($T_{\text{ant}} \propto G$), and low frequencies (< 100 MHz) associated with Galactic noise, meaning that even simple, cheap dipoles can span extraordinary usable bandwidth [20].

The total field of the array is determined by the vector addition of the fields radiated by the individual elements, and different beam shapes can be formed depending on the geometry of the array. This allows multibeaming (beamforming), i.e., combining signals from multiple elements so that multiple beams, each having a different orientation, can be simultaneously generated, acting as an additional observer. Multibeaming also provides the advantage of forming beams with shapes tailored to reduce noise. Examples of phased array radio telescopes are the Allen Telescope Array in Hat Creek, California (USA), the Deuterium Array in Westford, Massachusetts (USA), and the Long Wavelength Array Station 1 in central New Mexico (USA).

3.2.3 Interferometry: aperture synthesis

Radio wavelengths are orders of magnitude longer than optical wavelengths ($\frac{\lambda_{\text{radio}}}{\lambda_{\text{optical}}} \sim 10^9$). This means that diffraction effects are considerable, and thus angular resolution becomes affected when the dish diameter D reaches structural limitations. For example, consider a paraboloidal reflector of diameter 100 m [5]. Its resolution at the wavelength of 6 cm is comparable to that of the human eye in the visible spectrum(390 to 700 nm) [22]. Since it is of importance to precisely measure angular positions of stars and other cosmic objects, a new technique had to be developed in order to improve angular resolution. This mathematical signal processing technique is called aperture synthesis, a type of interferometry. The radio astronomers who developed this technique, Martin Ryle and Antony Hewish, shared the Nobel Prize for Physics in 1974 for such an important contribution.

Grosso modo, interferometers, the instruments used in aperture synthesis, cross-correlate received signals from widely separated antennas in an array. These signals are Fourier analyzed by other electronic devices to form an image having the same angular resolution that an instrument of the same size of the array would have. The actual signal processing is much more complex

[5] In fact, the largest single-aperture radio telescope is the Arecibo telescope, having a 305 m diameter dish.

and beyond the scope of this work; for details, see [46]. Examples of interferometers are the Very Large Array in central New Mexico (USA), the Atacama Large Millimeter/Submillimeter array (ALMA) in the Atacama Desert (Chile), The Giant Meterwave Radio Telescope (GMRT) in Pune (India), the LOw-Frequency ARray (LOFAR) distributed over Northern Europe, among others.

The resolution achieved by these instruments[6] compared to single-dish telescopes is impressive. Let us take as an example the ALMA telescope [52]. It consists of a giant array (66 dishes) of fifty-four 12-m antennas and twelve 7-m antennas, with baselines up to 16 km. The frequency range at which ALMA can observe is divided into bands, and data can only be taken in one band at a time. The bands span frequencies starting from 84 GHz and finishing at $\sim$ 950 GHz (λ $\sim$submilimiters to few millimeters). The spatial resolution that ALMA can achieve ranges from arcseconds[7] to milliarcseconds, depending on the configuration of the array (baseline length).

3.2.4 Future Prospects

One of the most important and ambitious projects for radio astronomy is the Square Kilometer Array (SKA) [17]. As its name says, the original purpose is to reach a 1 km^2 collecting surface, although its actual design projects it to largely exceed 1 km^2. It is designed to operate between 70 MHz and 10 GHz, and thus different antennas are needed to cover such bandwidth and to attain the desired level of resolution. This represents a new challenge, since innovative feeds and detectors must be introduced. However, that challenge could be overcome with machine learning techniques, as done by Gauci *et al.* [23]. In their study, they apply Genetic Algorithms (GA) to determine the most optimum configurations for the array of 250 (3000) dishes planned in the phase 1(2) of SKA, demonstrating the potential of machine learning techniques to help finding optimal antenna configurations.

[6]The angular resolution θ(radians) can be approximated by $\theta = \frac{\lambda}{B}$, where B is the baseline length.

[7]An arcsecond is approximately the angle subtended by a U.S. dime coin (18 mm) at a distance of 4 km. Taken from Wikipedia.

3.3 Astroparticle physics: antennas as particle detectors

Unlike radio astronomy, in astroparticle physics the desired radio signals are those whose sources are the interactions of ultra-high energy (UHE) astroparticles, such as cosmic rays and astrophysical neutrinos, with media in the Earth. These media can be air or dense media such as ice; or with the magnetic field of the Earth. These two are the Askaryan and geomagnetic effects, respectively. In this work we will focus on UHE neutrino (UHE-ν) detection only. The detection of UHE neutrinos would help to elucidate the nature of the astrophysical sources that create such particles and to serve as a test for particle physics at very high energies.

When UHE neutrinos interact with a medium, they produce a shower of secondary particles that contain a charge excess. If these charged particles move at a velocity greater than that of the light in the medium, they produce radio Cherenkov radiation, also known as Askaryan radiation. This phenomenon is known as Askaryan effect and will be described in the next subsection. While this effect contributes in both dense and non-dense media, the geomagnetic effect is negligible in dense media due to the compactness of the shower and is not relevant for neutrino detection in ice. Understanding the physics behind the Askaryan effect is fundamental for the design of antennas as particle detectors.

3.3.1 Electromagnetic shower and Askaryan effect

Consider an UHE electron neutrino ν_e entering the ice and undergoing a charged current interaction, $\nu_e + N \rightarrow e + N'$. Most of the energy that the ν_e originally had is transferred to the resulting electron. While passing through matter, the energy of the electron is degraded by interactions with the ice. Among the interactions that can happen to the high-energy electron, the most important is bremsstrahlung in the fields of the ice nuclei, since it has the largest cross section. After bremsstrahlung, which creates a secondary photon, the energy is (roughly) uniformly distributed between the electron and this secondary photon [28]. The secondary photon will create an electron-positron pair in interactions with other nuclei, as its cross section dominates at high energies, which will in turn interact to form more secondary particles. This iterative process produces an electromagnetic cascade shower that continues until the secondary particles reach energies at which the bremsstrahlung and ionization rates are equal. This energy is called the

critical energy E_c. Once this energy is reached, the remaining particles can likely undergo other processes besides bremsstrahlung and pair production, since their cross sections become equally important [39]. Among these processes, the main interaction channel for photons is Compton scattering ($\gamma + e^-_{\text{atom}} \rightarrow \gamma + e^-$), which degrades their momenta until they reach energies at which the photoelectric effect cross section is dominant, terminating the photons in the cascade shower. Electrons and positrons interact via Bhabha scattering ($e^+ + e^-_{\text{atom}} \rightarrow e^+ + e^-$), via positron annihilation ($e^+ + e^-_{\text{atom}} \rightarrow \gamma\gamma$), and via Møller scattering ($e^- + e^-_{\text{atom}} \rightarrow e^- + e^-$). Through these interactions, energy is deposited in the ice. The radius of a cylinder containing on average 90% of the shower's energy deposition is called the Molière radius R_{M}, and $R_{\text{M}} \sim 10$ cm in ice. Note that the interactions aforementioned contribute to a negative charge excess in the shower, either by annihilating positrons or adding electrons from the medium to the electromagnetic cascade. Monte Carlo simulations by Zas, Halzen and Stanev (ZHS) [53] and GEANT simulations [41, 42] predict the negative charge excess to be $\sim 20\%$ for shower energies > 1 PeV.

This 20% charge excess is not static in time. As the shower evolves, and the number of particles changes, the net charge grows reaching a maximum and then declines again. This can be understood as a time-varying "longitudinal current" [29], which, as we summarized in section 2.1, produces electromagnetic radiation, radially polarized and null in the center at the shower axis [2]. This radiation is also known as *Askaryan radiation*, named after Gurgen Askaryan, who postulated it in 1962 [6]. It was experimentally observed in 2001 using a silica sand target [43].

For wavelengths larger than the Molière radius in a dense medium, corresponding to frequencies $\lesssim 1$ GHz, the amplitudes of the fields add, producing a broadband (200 MHz-1.2 GHz) coherent radio pulse [6]. The energy of this coherent emission scales with the square of the charge excess in the shower, which is in turn linearly proportional to the energy of the incident particle E_ν. From this, the amplitude of the field scales as E_ν^2. This emission is maximal within a cone (Cherenkov cone) of half-angle θ_C satisfying $\cos\theta_C = 1/n$, where n is the refraction index of the medium and has a duration of less than a nanosecond [37]. For ice, $n = 1.78$, and thus $\theta_C \approx 57^\circ$.

Work by ZHS [53]; Alvarez-Muñiz, Vazquez and Zas [5]; Ralston and Buniy [13], Connolly and Hanson [27], among others, have allowed for the determination of a semi-analytic expression for the Askaryan field strength for different coherent zones (near-field, fresnel, far-field). This treatment also includes the LPM effect, which at high energies or high matter densities, increases the interaction length of the particles in the shower. All this is useful for UHE-ν experiments since it improves the Askaryan-signal template creation and facilitates threshold-sensitivity evaluation.

Given the nature of the Askaryan radiation, different collaborations have designed experiments to be able to detect such signals. This will be discussed in the next paragraphs.

3.3.2 UHE-ν experiments

The main goal of astroparticle experiments that use this radio technique is to measure the flux of cosmic rays and neutrinos at very high energies, such that astrophysical models can be confirmed or refuted. However, this task is very hard to perform since the flux falls off very quickly at such energies. Moreover, since neutrinos barely interact, their detection becomes much rarer and large interaction volumes are required. The number of neutrinos expected to be measured by an experiment depends on the fraction of neutrinos interacting in that volume that pass the trigger [16]. This is why enormous interaction volumes/areas are needed, which requires antenna arrays that can cover such volume/area, as well as necessitates sensitive antennas. Since radio wave observation by the antenna is the primary stage of this detection, an antenna design that improves the chances to observe such signal is crucial.

Various kinds of antennas are used for different UHE astroparticle experiments, as they provide different advantages in terms of adaptability to the experiment, sensitivity and cost. The ideal antenna should have no influence from temperature, humidity, and ground conditions, as some of them would be buried under Antarctic ice or endure some other extreme conditions. This is because gain behavior with changing environmental conditions is unknown [45]. Characteristics of each experiment are summarized in Table 1.

Here we give a brief description of the experiment and the antennas used for three different UHE neutrino experiments based in Antarctica: The Askaryan Radio Array (ARA), The

Antarctic Impulsive Transient Antenna (ANITA), and The Antarctic Ross Ice-Shelf ANtenna Neutrino Array (ARIANNA):

- **ARA** [3, 4]: This radio array has stations located inside the ice near the South Pole, at 200 m depth. Each station consists of 16 antennas, deployed along 4 strings of 4 antennas each, separated by ~ 10 m. Each station (separated by 2 km) acts as a single detector, and up to date three of them, out of the 37 planned, have been deployed. ARA will monitor the energy regime above $\sim 10^{17}$ eV.

  Allison *et al* [3] mention that the antenna array design must be such that the antennas can isotropically detect highly linearly polarized radio frequency (RF) impulses, for waves created either in distant sources (plane waves) or in closer sources (spherical waves). Regarding individual antennas, they should have a dipole-like response.

  In the current design, there are 2 types of antennas used: vertically polarized in-ice antennas (Vpol) and horizontally polarized in-ice antennas (Hpol). Two separated polarizations are chosen to be able to determine the polarization of the incoming signal, and subsequently use this information for neutrino reconstruction. The antennas used in ARA are birdcage dipoles for the Vpol and ferrite loaded quad-slot antennas (Fig. 5) for the Hpol, whose bandwidth is between 150 and 850 MHz (Fig. 4).

- **ANITA** [25, 49]: A balloon-borne antenna array flown at an altitude of 37 km containing 40 quad-ridged horn antennas. This balloon scans the Antarctic continent in a circumpolar trajectory, looking for Askaryan signals caused by neutrino interactions inside the Antarctic ice.

  The conceptual design, as stated by Gorham *et al.* in [25], requires the array of antennas to have a maximum coverage of the Antarctic ice beneath, broad radio spectral coverage and dual-polarization capability in order to maximize the background rejection and signal identification capabilities.

  To meet these requirements, the devices used by the ANITA experiment are highly directional, dual linearly-polarized horn antennas. The frequency range for the antennas is 0.3 to 1.2 GHz (Fig. 7) and the average full-width-at-half-maximum (FWHM) beamwidth 45°

	ARA	ANITA	ARIANNA
Antenna type	fat dipoles, slot-cylinder	quad-ridge dual-pol horns	LPDA
Frequency band [MHz]	150-850	300-1200	100-1000
Gain [dBi]	1-4	10	7-8
VSWR	$\lesssim$3.0:1	$\lesssim$1.5:1[9]	$\leq$2.0:1
Energy range [eV]	$10^{16} - 10^{19}$	$10^{18} - 10^{21}$	$10^{17} - 10^{19}$

Table 1: Comparison of detectors for different UHE-ν experiments

with a gain of approximately 10 dBi. The beam pattern, which is frequency-dependent, is narrow at high frequencies and wide at low frequencies.

- **ARIANNA** [18, 12, 10]: Deployed on the Ross Ice Shelf, it consist of stations with 8 downward facing antennas arranged in an octagonal shape at a depth of $\sim$ 2 m, spaced by $\sim$ 2 m. Since the Ross Ice Shelf is shielded by local mountains from radio background originated by nearby anthropogenic sources, the ARIANNA stations are designed to have minimal power consumption.

  The design concept of the ARIANNA detector is to deploy high-gain, directional antennas with a wide bandwidth in the range 100 MHz-1 GHz. Since the antennas will have two orientations, downward into the ice and upward, the directionality of the antennas will provide sensitivity for neutrinos and cosmic ray induced showers, respectively.

  To achieve these requirements, ARIANNA uses log-periodic dipole array (LPDA) antennas whose frequency response ranges from 105-1300 MHz (in air[8]) with a VSWR of 2.0:1 or less across the frequency band (Fig. 9). The forward gain was measured to be 7-8 dBi, with a front-to-back ratio of 15 dB. The half power angles are specified to be 60-70° in the E plane, and 110-130° in the H plane.

[8] In ice, the lower limit is shifted down to 80 MHz [24].
[9] Can be inferred from Fig. 7

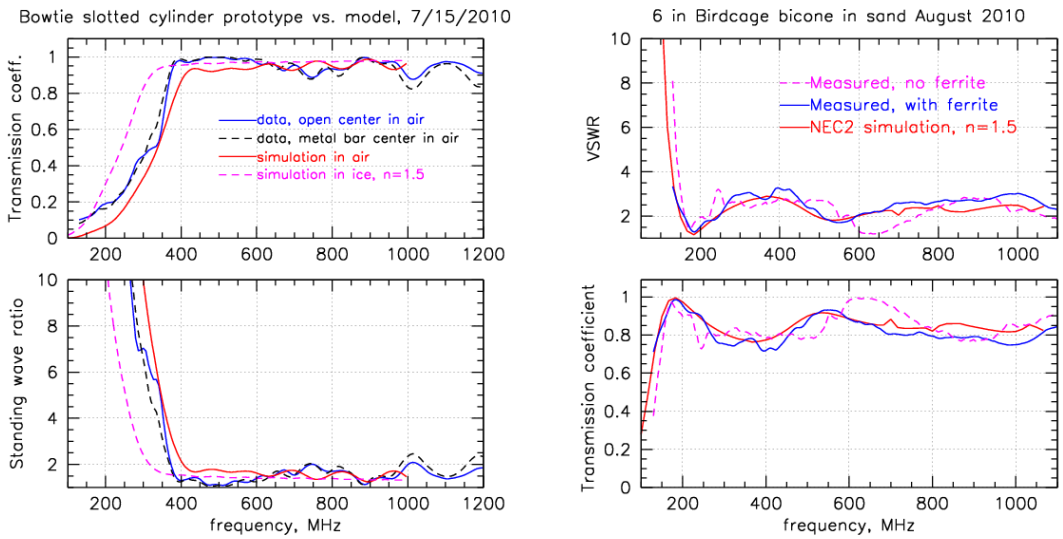

(a) Quad-slot (HPOL) (b) Birdcage bicone (VPOL)

Figure 4: The Voltage Standing Wave Ratio (top) and corresponding transmission coefficient (bottom) of the HPOL (left) and VPOL (right) antennas used by ARA. From [3]. The ferrite loading was added to lower the frequency response of the antennas.

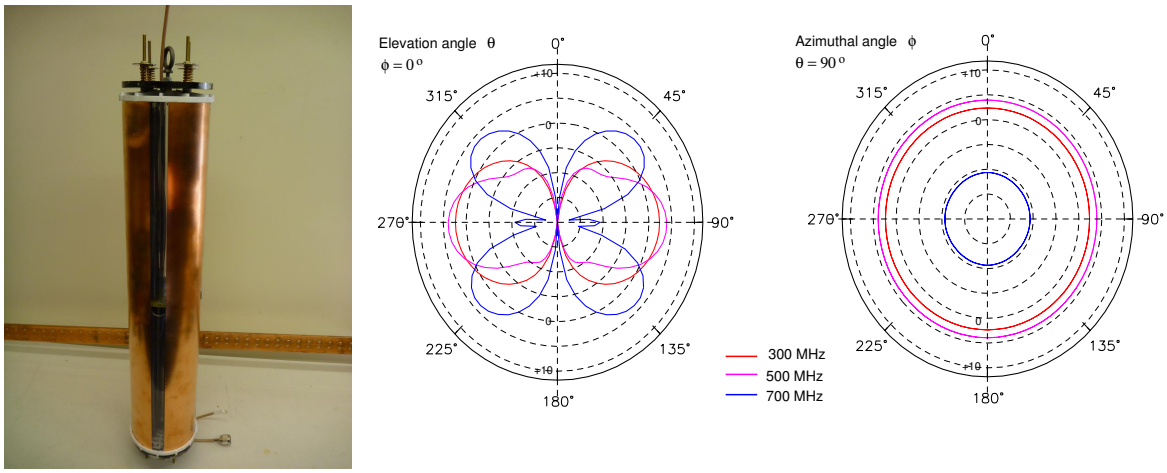

Figure 5: Simulated directional gain of a quad-slot antenna used in ARA. Taken from [3]. Note that a dipole-like response is shown by the antenna.

3.3.3 Future Prospects

So far, no UHE neutrinos have been detected using the radio-technique. There are many efforts ongoing to improve the chances to detect such particles, by both lowering the energy threshold and increasing the effective volume. In order to do so, the used antennas should have high-gain so that they can detect weak signals, since the electric field strength falls as $1/r$, where r is the

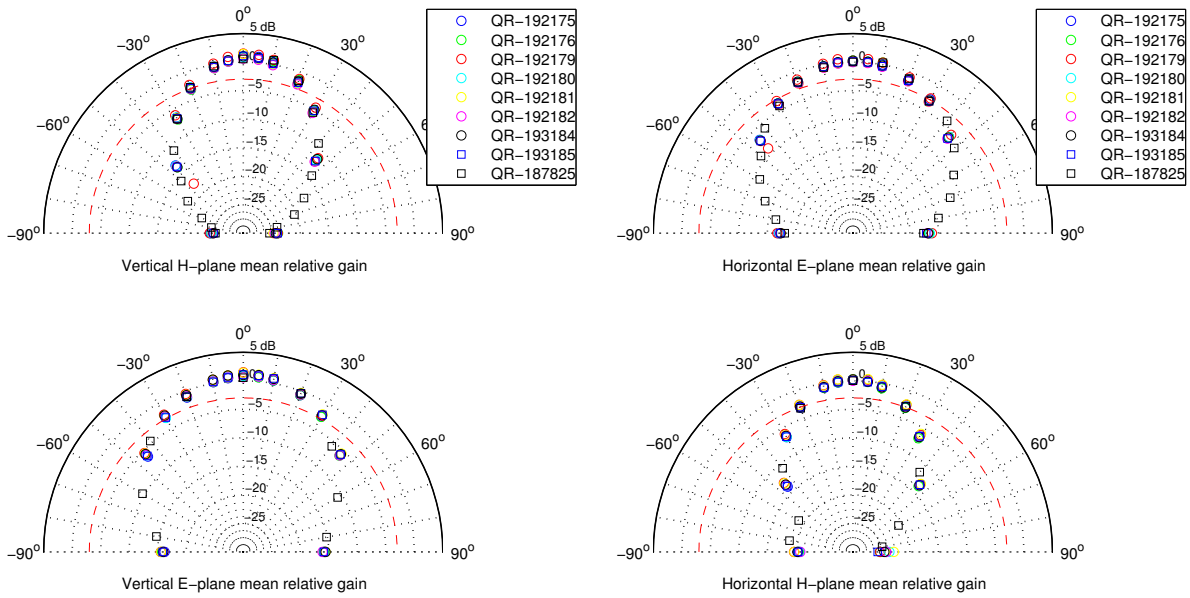

(a) ANITA antenna vertical polarization (b) ANITA antenna horizontal polarization

Figure 6: Measured directivity (in dB) relative to the pak gain for both E and $H-$planes for both antenna polarizations (vertical and horizontal). As stated in reference [25], the plotted data is the frequency-averaged gain for a flat-spectrum impulse across the 200-1200 MHz ANITA band for nine different horn antennas.

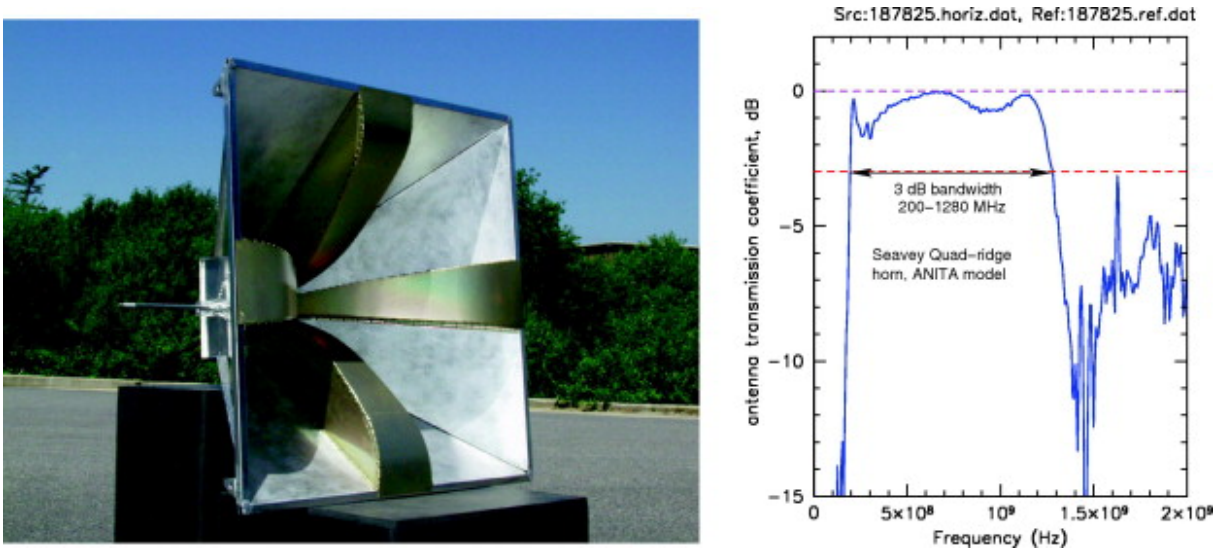

Figure 7: Left: one of the quad-ridged dual-polarization horn used by the ANITA experiment. Right: transmission coefficient as a function of frequency for the horn antenna. From [25].

distance between the neutrino interaction vertex and the antenna. Because the signal-to-noise ratio (SNR) is proportional to the gain, high-gain antennas lead to higher SNR values, which

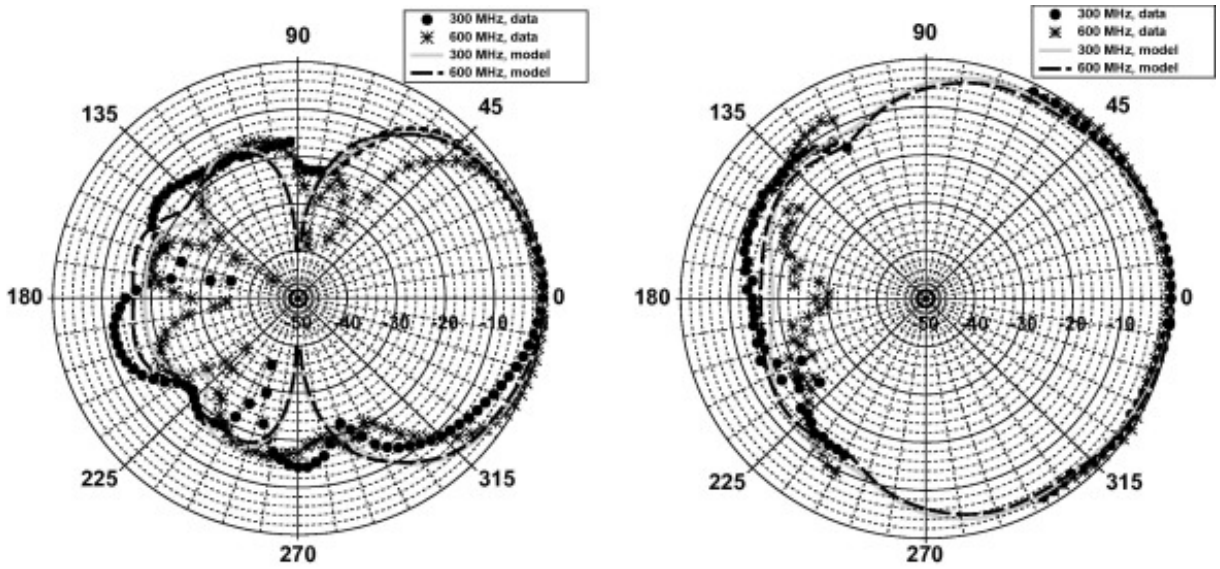

Figure 8: Measured and simulated beam pattern (normalized to 0 dB maximum) for one of the LPDA antennas used by the ARIANNA collaboration. The plotted gains are for 300 and 600 MHz. The left (right) figure is the E-(H-)plane radiation pattern. From [11]

increases the sensitivity, but they have a narrow angular coverage and may not fit the mechanical requirements to be deployed under ice, in a borehole. One approach for extending the angular coverage and increasing the effective gain is the in-ice phased array concept [48].

As in radio astronomy (cf. sec. 3.2.2), the advantage of *beamforming* is exploited in phased arrays. Individual antenna beam patterns would add up to cover a greater solid angle than a single antenna would, but with a higher gain, allowing to distinguish weak signals, produced by neutrino interactions, from noise, and consequently increasing the energy sensitivity (lowers the energy threshold).

Vieregg *et al.* state that the effective gain G_{eff} [dBi or dBd] of the phased array goes as

$$G_{\text{eff}} = 10 \log_{10}(N \times 10^{G/10}), \tag{3.1}$$

where N is the number of antennas, and G is the gain for each individual antenna (assuming they are identical) [dBi or dBd]. Note that $G_{\text{eff}} > G$ if $N > 1$. Avva *et al.* [7] estimate that this technique would increase the SNR as $\sim \sqrt{N}$. As an example, a 16-channel trigger array of dipole antennas would lower the experimental threshold by a factor of ~ 4. This initiative could

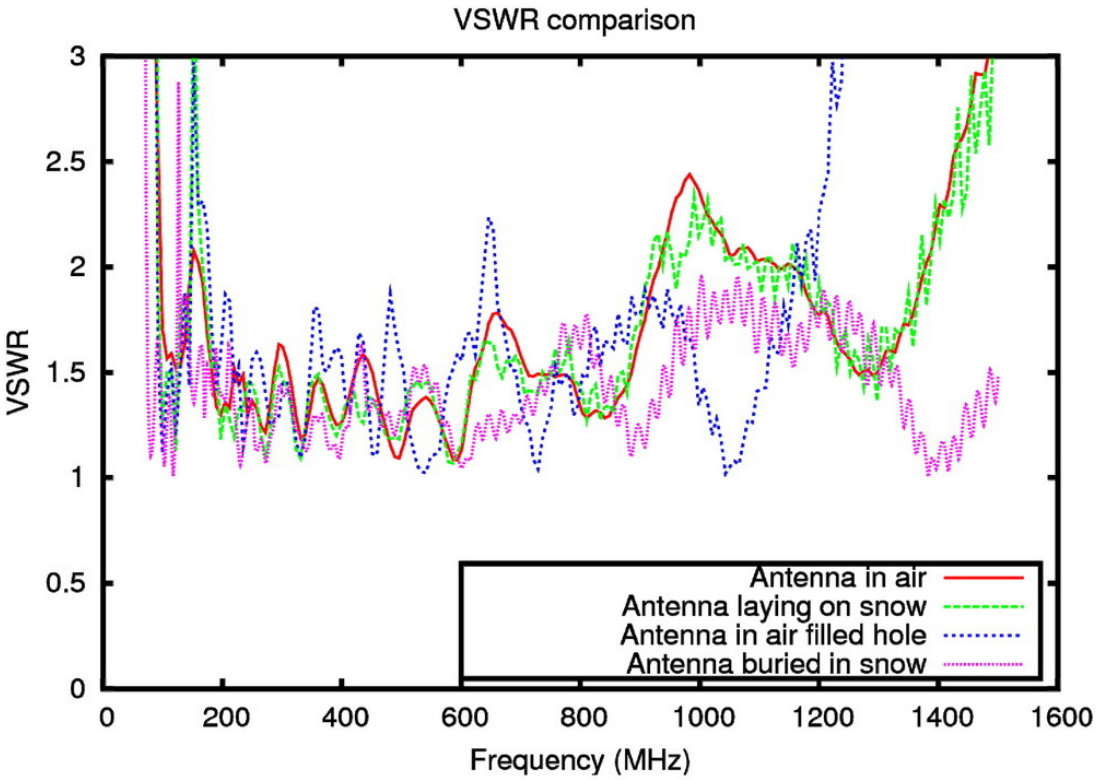

Figure 9: VSWR as a funciton of frequency in different scenarios for one of the LPDAs used by ARIANNA. From [24]. Note how the antenna response is improved for the antenna buried in snow.

be useful for current and future in-ice experiments, and is planned to be present in a recently proposed in-ice UHE-ν experiment: the Greenland Neutrino Observatory (GNO) [51]. In fact, ARA is deploying a phased array this fall, following the recommendations stated in [48, 7].

Another approach is to use brute force, i.e., to deploy a huge amount of antennas as is planned for The Giant Radio Array for Neutrino Detection (GRAND) [38]. The goal of GRAND is to use and array of $\sim 2 \times 10^5$ radio antennas over $\sim 2 \times 10^5\,\mathrm{km}^2$ in a low electromagnetic background, mountainous site. Unlike the UHE-ν experiments previously described, this proposed array is neither an in-ice experiment nor will it be in Antarctica. However, they use the same detection principle: Askaryan signals from air showers caused by ν_τ-produced decaying taus. GRAND aims at reaching a neutrino sensitivity as low as to ensure the detection of cosmogenic neutrinos above 3×10^{16} eV in the most pessimistic source models.

An array would be complicated for a balloon-borne experiment like ANITA. The only prac-

tical improvement that can be done for this kind of experiments is increasing the antenna gain. The ExaVolt Antenna (EVA), still under planning, would achieve that [26]. EVA plans to use a ~ 30 dBi antenna, ~ 3 times greater than that of the ANITA antennas, which would improve the sensitivity to neutrino-induced Askaryan signals by a factor >100 over any previous experiment [40]. The proposed design of EVA consists of a radio frequency (RF) reflector ring on the surface of a super-pressure ballon (SPB) and a feed array of receiving antennas inside it. The RF reflector ring would focus the signal to the interior of the balloon, similar to a reflector antenna. The major challenge of this project is on the mechanical side, since the array feed would be inside the balloon and could cause damage to it.

4 Conclusions

In this work we have superficially reviewed the physics behind radiation emission, and some of the parameters used to evaluate antenna performance and saw how they play a role in antenna design for the different application fields studied in this work: communications, radio astronomy and astroparticle physics (neutrino astronomy radio experiments, specifically).

From the literature, we could see that many efforts are underway to optimize and accelerate antenna design by using genetic algorithms (GAs), especially in the communications and radio astronomy fields. However, not much work has been done in astroparticle physics, which is expected since the radio technique is fairly new in this context. Fortunately, neutrino astronomy is quickly growing and then the GA area will soon have to be explored. This, along with other methods being currently developed such as phased arrays for in-ice experiments, will probably be the *"Veni, vidi, vici"* of neutrino astronomy at ultra-high energies, allowing the first detection of UHE-νs through radio methods.

References

[1] IEEE standard for definitions of terms for antennas. pages 1–50, March 2014.

[2] A. Aab, Abreu, et al. Probing the radio emission from air showers with polarization measurements. *Phys. Rev. D*, 89:052002, Mar 2014.

[3] P. Allison et al. Design and initial performance of the askaryan radio array prototype eev neutrino detector at the south pole. *Astroparticle Physics*, 35(7):457–477, 2 2012.

[4] P. Allison et al. Performance of two askaryan radio array stations and first results in the search for ultrahigh energy neutrinos. *Phys. Rev. D*, 93:082003, Apr 2016.

[5] J. Alvarez-Muniz, R. A. Vazquez, and E. Zas. Calculation methods for radio pulses from high-energy showers. *Phys. Rev.*, D62:063001, 2000.

[6] G. A. Askaryan. Excess negative charge of an electron-photon shower and its coherent radio emission. *Sov. Phys. JETP*, 14(2):441–443, 1962. [Zh. Eksp. Teor. Fiz.41,616(1961)].

[7] J. Avva et al. Development Toward a Ground-Based Interferometric Phased Array for Radio Detection of High Energy Neutrinos. 2016.

[8] J. Baars. *The Paraboloidal Reflector Antenna in Radio Astronomy and Communication: Theory and Practice*. Astrophysics and Space Science Library. Springer New York, 2007.

[9] C. A. Balanis. *Antenna Theory: Analysis and Design*. Wiley-Interscience, 2005.

[10] S. Barwick et al. A first search for cosmogenic neutrinos with the ARIANNA hexagonal radio array. *Astroparticle Physics*, 70:12 – 26, 2015.

[11] S. Barwick et al. Time-domain response of the ARIANNA detector. *Astroparticle Physics*, 62:139 – 151, 2015.

[12] S. W. Barwick et al. Design and performance of the ARIANNA HRA-3 neutrino detector systems. *IEEE Transactions on Nuclear Science*, 62(5):2202–2215, Oct 2015.

[13] R. V. Buniy and J. P. Ralston. Radio detection of high energy particles: Coherence versus multiple scales. *Phys. Rev. D*, 65:016003, Dec 2001.

[14] B. Burke and F. Graham-Smith. *An Introduction to Radio Astronomy*. Cambridge University Press, 2002.

[15] J. Cheng. *Fundamentals of Radio Telescopes*, volume 360. Springer, 2009.

[16] A. L. Connolly and A. G. Vieregg. Radio Detection of High Energy Neutrinos. 2016.

[17] P. E. Dewdney, P. J. Hall, R. T. Schilizzi, and T. J. L. W. Lazio. The square kilometre array. *Proceedings of the IEEE*, 97(8):1482–1496, Aug 2009.

[18] K. Dookayka. *Characterizing the Search for Ultra-High Energy Neutrinos with the ARIANNA Detector*. PhD thesis, University of California, Irvine, 2011.

[19] S. Ellingson. *Antennas in Radio Telescope Systems*. springer, 2014.

[20] S. W. Ellingson. Antennas for the next generation of low-frequency radio telescopes. *IEEE Transactions on Antennas and Propagation*, 53(8):2480–2489, Aug 2005.

[21] S. W. Ellingson. Sensitivity of antenna arrays for long-wavelength radio astronomy. *IEEE Transac-*

tions on Antennas and Propagation, 59(6):1855–1863, June 2011.

[22] S. Frey and L. Mosoni. A short introduction to radio interferometric image reconstruction. *New Astronomy Reviews*, 53(11):307 – 311, 2009. Proceedings: VLTI summerschool.

[23] A. Gauci, J. Abela, and K. Z. Adami. Optimal ska antenna configuration using genetic algorithms. In *2012 International Conference on Electromagnetics in Advanced Applications*, pages 1028–1031, Sept 2012.

[24] L. Gerhardt et al. A prototype station for arianna: A detector for cosmic neutrinos. *Nuclear Instruments and Methods in Physics Research Section A: Accelerators, Spectrometers, Detectors and Associated Equipment*, 624(1):85 – 91, 2010.

[25] P. Gorham et al. The antarctic impulsive transient antenna ultra-high energy neutrino detector: Design, performance, and sensitivity for the 2006-2007 balloon flight. *Astroparticle Physics*, 32(1):10 – 41, 2009.

[26] P. Gorham et al. The ExaVolt Antenna: A large-aperture, balloon-embedded antenna for ultra-high energy particle detection. *Astroparticle Physics*, 35(5):242 – 256, 2011.

[27] J. C. Hanson and A. L. Connolly. Complex analysis of askaryan radiation: A fully analytic treatment including the LPM effect and cascade form factor. *Astropart Phys*, 91:75–89, 2017.

[28] W. Heitler. *The Quantum Theory of Radiation*. Dover Books on Physics. Dover Publications, 1954.

[29] T. Huege and D. Besson. Radiowave Detection of Ultra-High Energy Neutrinos and Cosmic Rays. *ArXiv e-prints*, Jan. 2017.

[30] A. R. Jablon and R. K. Stilwell. Spacecraft reflector antenna development: Challenges and novel solutions. *Johns Hopkins APL Technical Digest*, 15(1), 1994.

[31] J. Jackson. *Classical Electrodynamics*. Wiley, 2007.

[32] S. R. Klein. A radio detector array for cosmic neutrinos on the ross ice shelf. *IEEE Transactions on Nuclear Science*, 60(2):637–643, April 2013.

[33] J. Kraus. *Antennas*. McGraw-Hill electrical and electronic engineering series. McGraw-Hill, 1950.

[34] J. Kraus. *Radio astronomy*. Cygnus-Quasar Books, 1984.

[35] J. D. Lohn, G. S. Hornby, and D. S. Linden. *An Evolved Antenna for Deployment on Nasa's Space Technology 5 Mission*, pages 301–315. Springer US, Boston, MA, 2005.

[36] T. Milligan. *Modern Antenna Design*. Wiley - IEEE. Wiley, 2005.

[37] P. Miočinović et al. Time-domain measurement of broadband coherent cherenkov radiation. *Phys. Rev. D*, 74:043002, Aug 2006.

[38] M. Olivier et al. The giant radio array for neutrino detection. *Epj Web Conf*, 135:02001, 2017.

[39] C. Patrignani et al. Review of Particle Physics. *Chin. Phys.*, C40(10):100001, 2016.

[40] C. Pfendner. The ExaVolt Antenna: Concept and Development Updates. In *European Physical Journal Web of Conferences*, volume 135 of *European Physical Journal Web of Conferences*, page 02002, Mar. 2017.

[41] S. Razzaque et al. Coherent radio pulses from geant generated electromagnetic showers in ice. *Phys. Rev. D*, 65:103002, May 2002.

[42] S. Razzaque et al. Addendum to "coherent radio pulses from geant generated electromagnetic showers in ice". *Phys. Rev. D*, 69:047101, Feb 2004.

[43] D. Saltzberg et al. Observation of the askaryan effect: Coherent microwave cherenkov emission from charge asymmetry in high-energy particle cascades. *Phys. Rev. Lett.*, 86:2802–2805, Mar 2001.

[44] F. G. Schröder. Radio detection of cosmic-ray air showers and high-energy neutrinos. *Prog Part Nucl Phys*, 93:1–68, 2017.

[45] F. G. Schröder. Review on Cosmic-Ray radio detection (VULCANO 2016). 2017.

[46] A. R. Thompson, J. M. Moran, and G. W. Swenson, Jr. *Interferometry and Synthesis in Radio Astronomy, 2nd Edition*. 2001.

[47] G. S. Varner. Radio detection of ultra high energy neutrinos. *Nucl Instruments Methods Phys Res Sect Accel Spectrometers Detect Assoc Equip*, 623(1):413–415, 2010.

[48] A. Vieregg, K. Bechtol, and A. Romero-Wolf. A technique for detection of pev neutrinos using a phased radio array. *Journal of Cosmology and Astroparticle Physics*, 2016(02):005, 2016.

[49] A. G. Vieregg. *The Search for Astrophysical Ultra-High Energy Neutrinos Using Radio Detection Techniques*. PhD thesis, University of California, Los Angeles, 2010.

[50] T. L. Wilson et al. *Practical Aspects of Filled Aperture Antennas*. springer, 2013.

[51] S. A. Wissel et al. Site Characterization and Detector Development for the Greenland Neutrino Observatory. *PoS*, ICRC2015:1150, 2016.

[52] A. Wootten and A. R. Thompson. The atacama large millimeter/submillimeter array. *Proceedings of the IEEE*, 97(8):1463–1471, Aug 2009.

[53] E. Zas, F. Halzen, and T. Stanev. Electromagnetic pulses from high-energy showers: Implications for neutrino detection. *Phys. Rev. D*, 45:362–376, Jan 1992.